

Mode-center Placement of Monolayer WS_2 in a Photonic Polymer Waveguide

Angelina Frank,^{*,†} Justin Zhou,^{*,‡} James A. Grieve,^{¶,†} Ivan Verzhbitskiy,[‡] José Viana-Gomes,[§] Leyi Loh,[‡] Michael Schmid,^{||} Kenji Watanabe,[⊥] Takashi Taniguchi,[#] Goki Eda,^{*,‡,@,Δ} and Alexander Ling^{†,‡}

[†]*Centre for Quantum Technologies, National University of Singapore, Singapore*

[‡]*Department of Physics, National University of Singapore, Singapore*

[¶]*Quantum Research Centre, Technology Innovation Institute, Abu Dhabi*

[§]*Departamento de Física, Centro de Física, Campus de Gualtar, Portugal*

^{||}*4th Physics Institute and Research Center SCoPE, University of Stuttgart, Germany*

[⊥]*Research Centre for Functional Materials, National Institute for Materials Science, Japan*

[#]*International Centre for Materials Nanoarchitectonics, National Institute for Materials Science, Japan*

[@]*Department of Chemistry, National University of Singapore, Singapore*

^Δ*Centre for Advanced 2D Materials, National University of Singapore, Singapore*

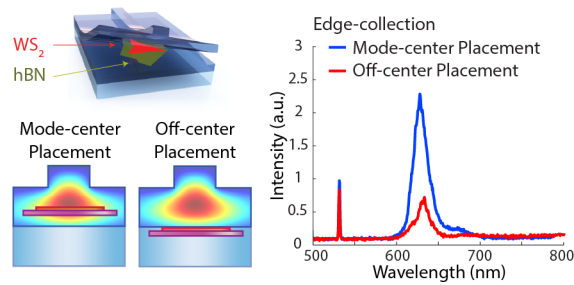
E-mail: angelina.frank@u.nus.edu; justinzhou@u.nus.edu; g.eda@nus.edu.sg

Abstract

Effective integration of 2D materials such as monolayer transition metal dichalcogenides (TMDs) into photonic waveguides and integrated circuits is being intensely pursued due to the materials' strong exciton-based optical response. Here, we present a platform where a WS_2 -hBN 2D heterostructure is directly integrated into the photonic mode-center of a novel polymer ridge waveguide. FDTD simulations and collection of

photoluminescence from the guided mode indicate that this system exhibits significantly improved waveguide-emitter coupling over a previous elastomer platform. This is facilitated by the platform’s enhanced refractive-index contrast and a new method for mode-center integration of the coupled TMD. The integration is based on a simple dry-transfer process that is applicable to other 2D materials, and the platform’s elastomeric nature is a natural fit to explore strain-tunable hybrid-photonic devices. The demonstrated ability of coupling photoluminescence to a polymer waveguide opens up new possibilities for hybrid-photonic systems in a variety of contexts.

TOC Graphic



Introduction

Monolayer transition metal dichalcogenides (TMDs) are a material class of great interest due to their exciton-based optical properties in both linear and non-linear regimes.¹⁻⁴ They have also been shown capable of hosting single-photon emitters.⁵⁻⁷ Besides the tunability of their bandgap in response to electric fields,^{8,9} TMDs’ exciton dynamics can be further modified through stacking into van der Waals heterostructures,¹⁰ chemical doping,¹¹ and application of mechanical strain.¹² These properties are of particular interest in the context of Photonic Integrated Circuits (PICs) where the goal is to couple a photon-routing structure to elements with strong and tunable optical response.¹³ Such circuits find applications in

optical communication,¹⁴ computation¹⁵ and sensing.^{16–18} Integration of TMDs into photonic waveguides can be readily achieved by direct transfer, taking advantage of the material’s van der Waals bonding nature.^{19,20} To date, most hybrid systems with an optically coupled 2D material realize placement away from the photonic mode maximum (off-center placement) or at a dielectric interface, e.g. close to an exposed fiber core,^{21,22} at the end-face of an optical fiber,²³ or on top of a waveguide in integrated photonics.^{24–28}

Previously, we have demonstrated integration of a TMD into an elastomeric ridge waveguide.²⁹ However, the optical coupling efficiency in this system was limited by the material’s off-center placement in between high- and low-refractive index layers and a relatively low index contrast ($n_1 - n_2 \sim 0.001$). Addressing this limited coupling efficiency is desirable, since elastomeric waveguides are an exciting platform for hybrid photonic systems due to elasticity, as well as a simple, mild and fast fabrication cycle that is cost effective and favours integration with additional micro- and nanostructures. Potential applications include a.o. rapid-prototyping, foundational material studies and lab-on-a-chip systems.^{30–34} An additional advantage is the environmental shielding that encapsulation provides for emitters.

Here, we present a novel elastomer ridge waveguide together with a new technique to integrate a 2D heterostructure (WS₂-hBN) in the mode-center of the waveguide (Figure 1 a). The device displays markedly enhanced emitter-mode coupling compared to the previous elastomer platform. The enhancement relies on two factors. Firstly, the newly developed system employs two (commercially available) polymer formulations that increase the index contrast by two orders of magnitude ($n_1 - n_2 \sim 0.1$). As a result, the platform can be miniaturized, reducing the effective mode area by a factor of ~ 20 from $166.4 \mu\text{m}^2$ for the previous platform down to $8.5 \mu\text{m}^2$. This concentration of the electromagnetic field facilitates interaction between material and guided mode, while simultaneously increasing the waveguide’s collection efficiency. Secondly, a new fabrication sequence allows for placement of a 2D material in the mode center. This contrasts with the previous method where a 2D material could only be placed off-center, i.e. between the high- and low-index polymer. Therefore,

emission from integrated 2D materials which arises from in-plane dipole sources³⁵ couples more effectively to the guided mode in the new device. Numerical simulations (FDTD, Lumerical) indicate that this miniaturization and optimized placement lead to an overall improvement of the mode overlap compared to the previous system, and that mode-center placement causes improvement by a factor of 20 compared to off-center placement in the new platform (Figure 1 b and c). This position serves as a benchmark, as it would be the most strongly coupling configuration realizable without the introduced fabrication method. We provide an experimental comparison between mode-center and off-center placement and confirm the improved interaction between mode and 2D material via collection of top-down-excited (free-space-excited) photoluminescence from the guided mode (edge-collection). This collection evidences significant enhancement compared to the previous platform where no signal was observable via edge-collection.

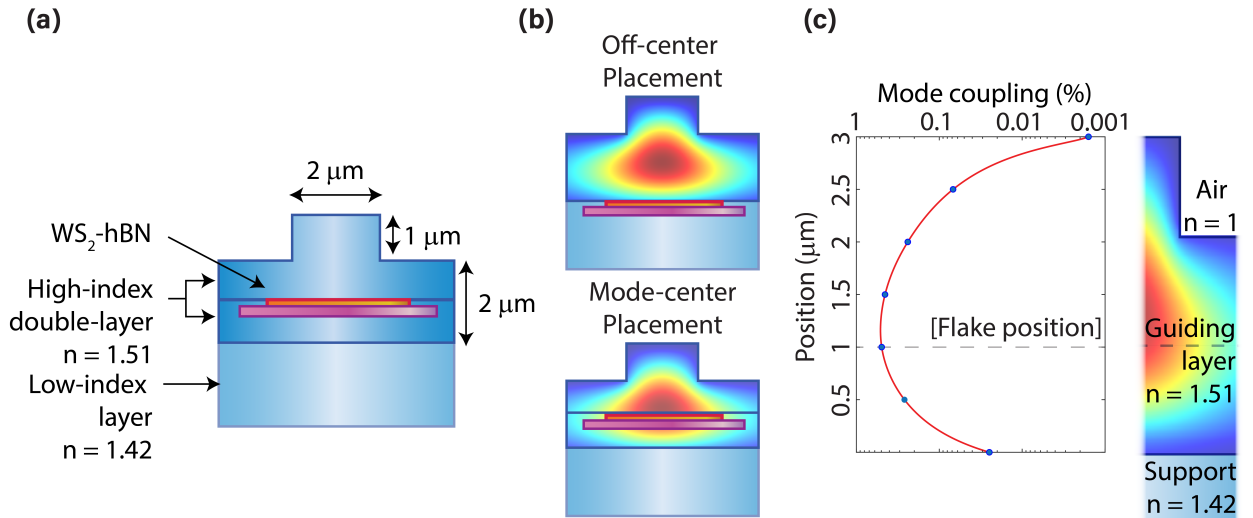


Figure 1: (a) Schematic depiction of the waveguide with the integrated $\text{WS}_2\text{-hBN}$ heterostructure (thickness $\sim 20\ \text{nm}$) (b) Illustration of off- and mode-center placement (emitter not drawn to scale) together with the mode profile. (c) Simulation of a dipole source's emission at $620\ \text{nm}$ coupling to the waveguide's fundamental mode for different vertical positioning. A maximum mode coupling of $0.49\ \%$ in one propagation direction is predicted. The red line is intended as a guide to the eye.

Experimental

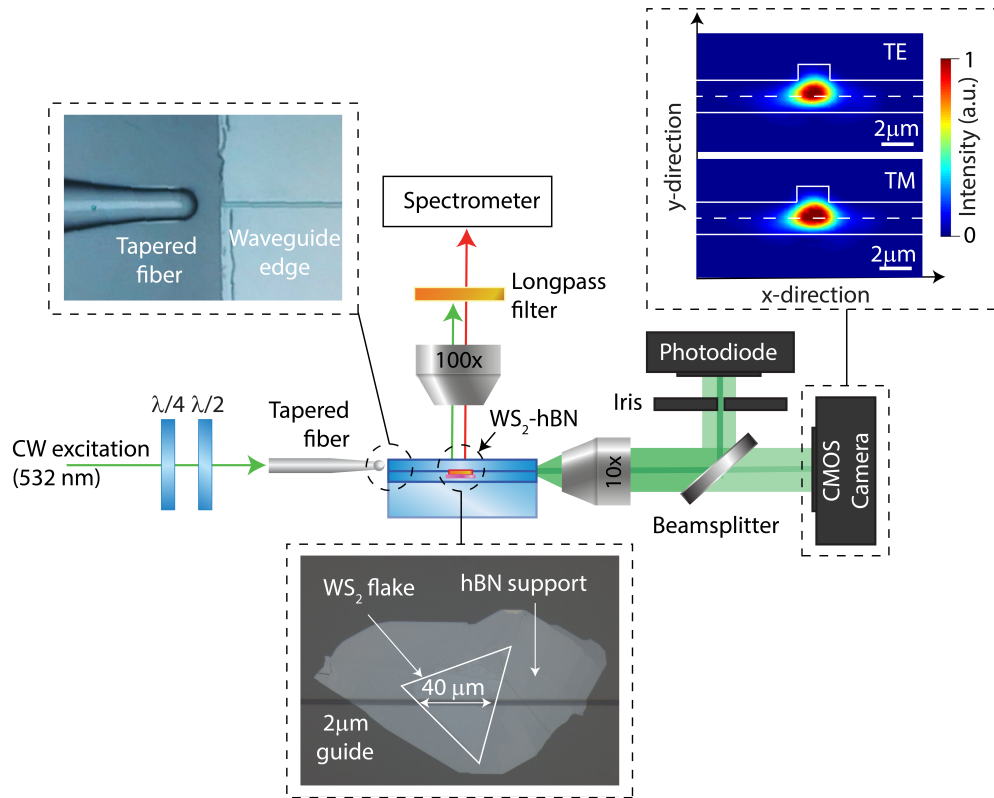


Figure 2: Schematic of the experimental setup configured for edge-excitation with a 532 nm pump laser and collection of photoluminescence from free space. Top left: Microscope image of a tapered fiber aligned to the waveguide for edge-coupling. Top right: Recorded images of the waveguide’s output profile for orthogonal pump polarizations. White lines schematically outline the waveguide. Bottom: Microscope image of the WS_2 -hBN heterostructure within the waveguide. WS_2 is contained within the white lines.

The developed polymer platform is a ridge waveguide based on two polymers ($n_1 \sim 1.42$ and $n_2 \sim 1.51$ at 532 nm). Integration into the mode-center is achieved via dry-transfer of a WS_2 -hBN heterostructure onto a waveguide precursor and subsequent plasma-bonding of two pre-cured polymer layers that make up the lower and the upper half of the high-refractive-index layer (see Methods for details). Each half of this guiding layer is about 1 μm thick and the waveguide ridge has a width of 2 μm with a height of 1 μm (Figure 1a). The structure is capable of single-mode guiding orthogonal polarizations equally (Figure 2, top left). The refractive index difference between guiding polymer layer and the supporting polymer matrix

lies between 0.085 to 0.1 and is stable over a range of wavelengths and temperatures as measured by a critical angle refractometry^{36,37} (see Supporting Information).

A schematic of the experimental setup configured for an edge-coupled pump (edge-excitation) is shown in Figure 2. The polymer substrate is approximately 1.3 cm in length and the WS₂-hBN heterostructure is placed close to the center of the device. Here, hBN with a thickness of 20 nm serves as structural support to prevent wrinkling. The WS₂ monolayer covers a length of 40 μm along the waveguide. Fiber, waveguide and collection optics are each mounted onto three- and five-axis translation stages (ULTRAlign, Newport) for alignment. A lensed single-mode fiber (SM-630-HP, conical taper: 1.6-2 μm) is edge-coupled on one side and either connected to a spectrometer (NTegra system by NT-MTD) or to a 532 nm pump. A 100x microscope objective (Olympus, 0.6 NA) is focussed onto WS₂ from the top and connected to either a spectrometer or a 532 nm light source. We linearize the polarization of the edge-coupled fiber using a polarizer, half-wave plate (HWP) and quarter-wave plate (QWP), with the latter pre-compensating for birefringence in the fiber. The edge of the waveguide chip is imaged onto a CMOS camera using a 10x objective lens to facilitate and monitor fiber alignment. An additional non-polarizing beam splitter in this optical collection path allows for simultaneous monitoring of both the transmitted output profile and the transmitted power via a power meter. An iris ensures that only the guided mode's intensity evolution is recorded. All experiments were performed at room-temperature.

Results

To characterize optical material-waveguide coupling in the device, we employed FDTD simulations and different excitation-collection schemes as outlined below. Initially, we estimated how much of the modal power flow (i.e. the Poynting vector along propagation direction) overlaps with the material for different vertical WS₂ placements inside the waveguide. Modelling WS₂ as a 1 nm thick and 3 μm wide area perpendicular to the direction of mode

propagation, we calculated a fractional power flow of 0.055% through the TMD for mode-center placement in contrast to $6.03 \times 10^{-5}\%$ for surface placement and 0.0021% for placement below the photonic mode i.e. at the interface between high- and low-index polymer which we refer to as off-center placement below. This corresponds to an enhancement of the overlap by almost three orders of magnitude compared to surface placement and one order of magnitude compared to off-center placement.

We first confirmed emitter-waveguide coupling by exciting the material from the top and collecting its photoluminescence (PL) from the guided mode via edge-collection (Figure 3). The detection of excitonic PL here is an important illustration of the device’s improved material-guide coupling since the previous system did not show a signal in this configuration.²⁹ In these experiments, we moved the excitation spot along the waveguide-region covered by WS_2 and recorded the edge-collected PL for two different devices that realize either mode-center placement or off-center placement (with a material offset from the mode center by $1 \mu\text{m}$). We note that edge-collection of PL from the waveguide mode is possible for

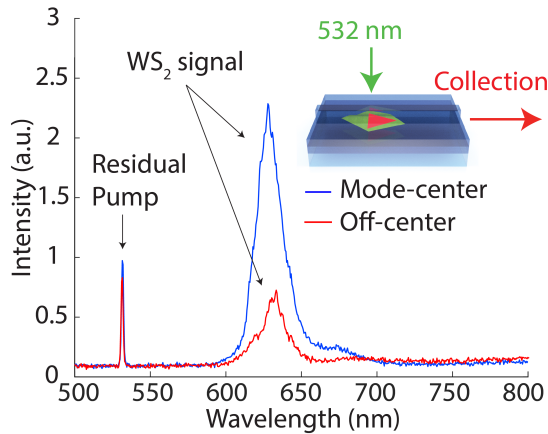


Figure 3: Edge-collected WS_2 photoluminescence from the guided mode in the developed waveguide system. (a) The stronger WS_2 photoluminescence coupled to the waveguide via mode-center placement (blue) indicates its superior mode-coupling compared to off-center placement (red) (integration time = 30 s, $350 \mu\text{W}$ pump).

both the mode-center and the off-center device. The difference in coupling predicted to arise from the optimized mode-center placement is indeed observable as a higher average signal.

In this configuration, however, a rigorous quantitative evaluation of the relative coupling efficiency is not possible due to setup limitations, and will be subject of future studies.

To investigate the relative performance of the mode-center and off-center device more closely, we established a second experimental configuration where excitation and collection points are interchanged such that we recorded the PL emitted into free space upon excitation by an edge-coupled pump (Figure 4 and 5). Using an excitation power of $40 \mu\text{W}$ ensures that we stay within the linear regime of WS_2 exciton emission. In this range, the collected PL intensity will be proportional to the excitation rate and serve as a measure of how well the waveguide mode couples to WS_2 . We compared the coupling for mode-center placement with that for off-center placement. To account for local variations in the material's quantum yield, we normalized the PL against the top-down excited and -collected PL at every site. Further, we collected the emission every $2.1 \mu\text{m}$ along the waveguide where it is interfaced with the flake (Figure 4 a). As anticipated, the mode-center device shows a markedly stronger response compared to the off-center device under the same excitation conditions (Figure 4). Moreover, we observed nearly exponential decay of the signal along the channel, indicating extinction of the waveguide mode. We measured an overall signal ratio of 11:1 for mode-center compared to off-center placement. This is evidence for the anticipated facilitation of coupling through mode-center placement, with simulations predicting a ~ 20 -times enhancement. The difference between simulation and experiment may be due to the dielectric properties of the 20 nm thick hBN support which were not included in the model.

Lastly, to confirm that WS_2 -hBN maintains its structure and that the waveguide is, in fact, polarization-preserving, we recorded the PL in the same scheme but under variation of the pump polarization and at a fixed collection site (Figure 5). This yielded an expected polarization dependence of the PL signal, with an intensity that is minimal for out-of-plane-polarized pump light. The polarization dependence is due to the strictly in-plane orientation of excitons.³⁵ The extinction ratio, that is, the ratio of the PL intensity

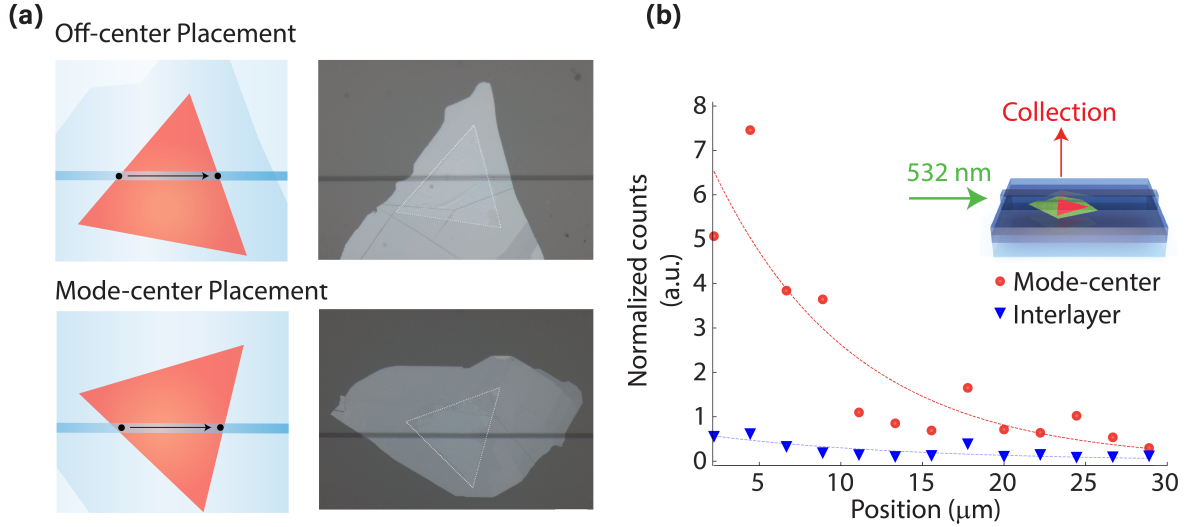


Figure 4: Experimental comparison of mode coupling for WS₂-hBN integrated in the mode-center and off-center. (a) The photoluminescence of WS₂ excited by the photonic mode is collected from free-space at different positions along the waveguide (black dots). (b) Plot of the free-space collected photoluminescence at different positions normalized for local variations in the quantum yield. A least-square exponential fit reveals that the extinction coefficients are similar (0.08 and 0.12) and integration of the counts shows a distinctively higher excitation ratio of 11:1 for mode-center compared to off-center placement.

for in-plane and out-of-plane polarized excitation, was found to be ~ 65 , indicative of this waveguide’s polarization-preserving characteristics. It also serves as a confirmation of the material’s preserved structure throughout fabrication and transfer. A slight asymmetry in the polarization plot originates from experimental imperfections.

Weaker coupling of dipole radiation to the waveguide compared to this free-space-collected emission is expected for a dipole oriented in-plane with a Poynting vector that has an angular distribution largely consisting of out-of-plane components. The radiation pattern shows little overlap with the waveguide mode, evoking a weaker signal compared to that collected as free-space radiation.

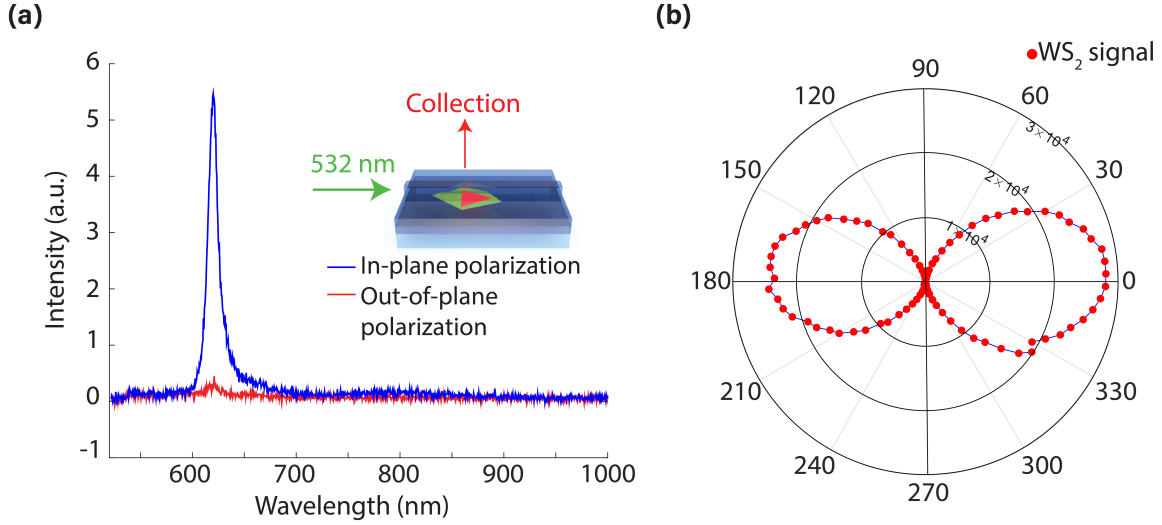


Figure 5: WS_2 photoluminescence excited by an edge-coupled pump and measured via free-space collection. Out-of-plane polarized light shows minimal interaction with WS_2 . (a) In-plane and out-of-plane polarized pump light couples to the waveguide and evokes different photoluminescence signals. This confirms different interaction cross-sections with the dipole-moment of two-dimensional materials. (b) Polar plot of the PL signal's integrated intensity at different pump polarizations.

Conclusion

We have demonstrated a new elastomeric hybrid photonic platform where light-matter interaction with WS_2 -hBN, a 2D heterostructure, is facilitated by miniaturization of the waveguide and mode-center integration of the material. Simulations and experiments confirm that the system exhibits significantly enhanced interaction between the encapsulated material and waveguide compared to a previous platform. Most notable is the newly gained ability to detect guide-coupled photoluminescence. The dry-transfer technique used for integration is applicable to other two-dimensional material systems.

While semiconductor platforms such as silicon-nitride waveguides can offer higher coupling efficiencies of $\sim 7\%$ ²⁴ due to a higher index-contrast ($n_{\text{Si}_3\text{N}_4} = 2.055$, $n_{\text{SiO}_2} = 1.461$ at 532 nm)^{38,39} and smaller mode area (of $\sim 0.14 - 0.2 \mu\text{m}^2$), the presented polymer platform offers unique features such as strain-tunability, low fabrication costs, a short development time, and a simple fabrication procedure. Mild curing conditions also enable versatile approaches

to material integration. Besides fundamental studies of TMDs, and other 2D materials, we believe that this system will be of interest in the context of microfluidics, chemical-tuning, flexible photonics, optoelectronic devices, and encapsulation of other nano- and micro-scale materials into polymeric waveguides for novel hybrid systems. While a higher refractive-index contrast of the materials is desirable for further miniaturization of the platform e.g. to build on-chip interferometers and multi-component circuits, the newly demonstrated ability to couple photoluminescence to the waveguide facilitates applications where 2D materials may also be used as integrated (non-)linear and (non-classical) light sources in the near-room-temperature regime.

Methods

Heterostructure Fabrication and Transfer

The WS₂-hBN heterostructure was assembled using a pick-up technique. WS₂ monolayers were first grown onto Si substrates via a liquid-mediated chemical vapor deposition method. hBN flakes were tape-exfoliated from bulk hBN crystals supplied by National Institute for Materials Science (NIMS), Japan, onto polydimethylsiloxane (PDMS) substrates (Sylgard184, Dow). These hBN flakes were subsequently used to pick-up the CVD-grown WS₂ flakes. During the pick-up, the WS₂ samples were heated to 130 °C to facilitate the pick-up process. Lastly, the WS₂-hBN heterostack was released onto the waveguide using a dry-transfer technique.

Waveguide Fabrication

Waveguides are fabricated from two different PDMS formulations (Sylgard184 and Gelest OE50) on two silicon wafers. To create the waveguide ridge with mode-center placement, a silicon wafer is spin-coated with a 1 μm thick layer of positive photoresist (AZ1512). The waveguide pattern is laser-written into this layer. Gelest OE50 is spin-coated onto this

mold to a thickness of $\sim 1 \mu\text{m}$. The wafer is cured at $55 \text{ }^\circ\text{C}$ for 4 hrs and the TMD-hBN heterostructure is transferred via soft lithography, making up the first half of the guiding layer. A second, unpatterned photoresist-coated substrate is prepared again by spin-coating and curing a $1 \mu\text{m}$ thick layer of GelestOE50 on the AZ-coated wafer. A 2 mm thick layer of Sylgard184 (the lower-refractive index polymer) is cured on top of this second substrate at $70 \text{ }^\circ\text{C}$ for 1 hr. This substrate now contains the lower part of the guiding layer (Gelest OE50) and its support matrix (Sylgard184). After treatment with oxygen plasma for 30 seconds, the two halves are brought in contact, forming a permanent bond and completing the structure. For off-center placement, we increase the thickness of the high-index polymer-layer to $2 \mu\text{m}$, transfer WS_2 -hBN of the same dimensions as for the mode-center device onto it and plasma-bond the layer directly to the low-index polymer.

Acknowledgement

A.L acknowledges support by the National Research Foundation, Prime Minister’s Office, Singapore. G.E. acknowledges support from the Ministry of Education (MOE), Singapore, under AcRF Tier 3 (MOE2018-T3-1-005) and the Singapore National Research Foundation for funding the research under the medium-sized center program. The authors thank Prof. Harald Giessen for the helpful correspondence and for facilitating material characterization and thank Isa Ahmadalidokht for fruitful discussions.

Supporting Information Available

Refractive Index Measurements

Refractive indices of the polymers were measured using a commercially available critical-angle refractometer (Schmidt-Haensch, ATR-L).

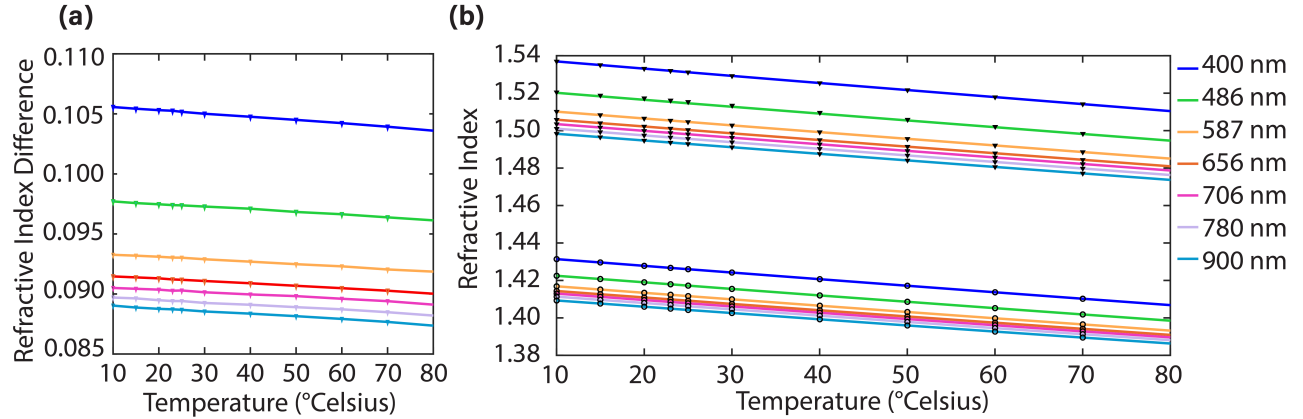


Figure 6: (a) Refractive index difference between high- and low-index polymer (b) Refractive index measurements for the used polymers. Range 1.44-1.38: Sylgard 184; Range 1.54 - 1.47: Gelest OE50.

References

- (1) Malard, L. M.; Alencar, T. V.; Barboza, A. P. M.; Mak, K. F.; de Paula, A. M. Observation of Intense Second Harmonic Generation from MoS₂ Atomic Crystals. *Physical Review B* **2013**, *87*, 201401.
- (2) Yin, X.; Ye, Z.; Chenet, D. A.; Ye, Y.; O'Brien, K.; Hone, J. C.; Zhang, X. Edge Nonlinear Optics on a MoS₂ Atomic Monolayer. *Science* **2014**, *344*, 488–490.
- (3) Mak, K. F.; Shan, J. Photonics and Optoelectronics of 2D Semiconductor Transition Metal Dichalcogenides. *Nature Photonics* **2016**, *10*, 216–226.
- (4) Sun, Z.; Martinez, A.; Wang, F. Optical Modulators with 2D Layered Materials. *Nature Photonics* **2016**, *10*, 227–238.
- (5) Srivastava, A.; Sidler, M.; Allain, A. V.; Lembke, D. S.; Kis, A.; Imamoglu, A. Optically Active Quantum Dots in Monolayer WSe₂. *Nature Nanotechnology* **2015**, *10*, 491–496.
- (6) Koperski, M.; Nogajewski, K.; Arora, A.; Cherkez, V.; Mallet, P.; Veuillen, J.-Y.; Marcus, J.; Kossacki, P.; Potemski, M. Single Photon Emitters in Exfoliated WSe₂ Structures. *Nature Nanotechnology* **2015**, *10*, 503–506.

- (7) Tran, T. T.; Choi, S.; Scott, J. A.; Xu, Z.-Q.; Zheng, C.; Seniutinas, G.; Bendavid, A.; Fuhrer, M. S.; Toth, M.; Aharonovich, I. Room-Temperature Single-Photon Emission from Oxidized Tungsten Disulfide Multilayers. *Advanced Optical Materials* **2017**, *5*, 1600939.
- (8) Chu, T.; Ilatikhameneh, H.; Klimeck, G.; Rahman, R.; Chen, Z. Electrically Tunable Bandgaps in Bilayer MoS₂. *Nano Letters* **2015**, *15*, 8000–8007.
- (9) Wang, Q. H.; Kalantar-Zadeh, K.; Kis, A.; Coleman, J. N.; Strano, M. S. Electronics and Optoelectronics of Two-Dimensional Transition Metal Dichalcogenides. *Nature Nanotechnology* **2012**, *7*, 699–712.
- (10) Rivera, P.; Yu, H.; Seyler, K. L.; Wilson, N. P.; Yao, W.; Xu, X. Interlayer Valley Excitons in Heterobilayers of Transition Metal Dichalcogenides. *Nature Nanotechnology* **2018**, *13*, 1004–1015.
- (11) Mouri, S.; Miyauchi, Y.; Matsuda, K. Tunable Photoluminescence of Monolayer MoS₂ via Chemical Doping. *Nano Letters* **2013**, *13*, 5944–5948.
- (12) Castellanos-Gomez, A.; Roldán, R.; Cappelluti, E.; Buscema, M.; Guinea, F.; van der Zant, H. S. J.; Steele, G. A. Local Strain Engineering in Atomically Thin MoS₂. *Nano Letters* **2013**, *13*, 5361–5366.
- (13) Elshaari, A. W.; Pernice, W.; Srinivasan, K.; Benson, O.; Zwiller, V. Hybrid Integrated Quantum Photonic Circuits. *Nature Photonics* **2020**, *14*, 285–298.
- (14) Sibson, P.; Erven, C.; Godfrey, M.; Miki, S.; Yamashita, T.; Fujiwara, M.; Sasaki, M.; Terai, H.; Tanner, M. G.; Natarajan, C. M.; Hadfield, R. H.; O’Brien, J. L.; Thompson, M. G. Chip-Based Quantum Key Distribution. *Nature Communications* **2017**, *8*, 13984.

- (15) Flamini, F.; Spagnolo, N.; Sciarrino, F. Photonic Quantum Information Processing: A Review. *Reports on Progress in Physics* **2018**, *82*, 016001.
- (16) Chamanzar, M.; Xia, Z.; Yegnanarayanan, S.; Adibi, A. Hybrid Integrated Plasmonic-Photonic Waveguides for on-Chip Localized Surface Plasmon Resonance (LSPR) Sensing and Spectroscopy. *Optics Express* **2013**, *21*, 32086–32098.
- (17) Kohler, D.; Schindler, G.; Hahn, L.; Milvich, J.; Hofmann, A.; Länge, K.; Freude, W.; Koos, C. Biophotonic Sensors with Integrated Si₃N₄-Organic Hybrid (SiNOH) Lasers for Point-of-Care Diagnostics. *Light: Science & Applications* **2021**, *10*, 64.
- (18) Porcel, M. A. G.; Hinojosa, A.; Jans, H.; Stassen, A.; Goyvaerts, J.; Geuzebroek, D.; Geiselmann, M.; Dominguez, C.; Artundo, I. Silicon Nitride Photonic Integration for Visible Light Applications. *Optics & Laser Technology* **2019**, *112*, 299–306.
- (19) Tonndorf, P.; Del Pozo-Zamudio, O.; Gruhler, N.; Kern, J.; Schmidt, R.; Dmitriev, A. I.; Bakhtinov, A. P.; Tartakovskii, A. I.; Pernice, W.; Michaelis de Vasconcellos, S.; Bratschitsch, R. On-Chip Waveguide Coupling of a Layered Semiconductor Single-Photon Source. *Nano Letters* **2017**, *17*, 5446–5451.
- (20) Joshi, S.; Kaushik, B. K. Transition Metal Dichalcogenides Integrated Waveguide Modulator and Attenuator in Silicon Nitride Platform. *Nanotechnology* **2020**, *31*, 435202.
- (21) Ngo, G. Q. et al. Scalable Functionalization of Optical Fibers using Atomically Thin Semiconductors. *Advanced Materials* **2020**, *32*, 2003826.
- (22) Zuo, Y. et al. Optical Fibres with Embedded Two-Dimensional Materials for Ultrahigh Nonlinearity. *Nature Nanotechnology* **2020**, *15*, 987–991.
- (23) Vogl, T.; Lu, Y.; Lam, P. K. Room Temperature Single Photon Source using Fiber-Integrated Hexagonal Boron Nitride. *Journal of Physics D: Applied Physics* **2017**, *50*, 295101.

- (24) Peyskens, F.; Chakraborty, C.; Muneeb, M.; Van Thourhout, D.; Englund, D. Integration of Single Photon Emitters in 2D Layered Materials with a Silicon Nitride Photonic Chip. *Nature Communications* **2019**, *10*, 4435.
- (25) He, J. et al. Low-Loss Integrated Nanophotonic Circuits with Layered Semiconductor Materials. *Nano Letters* **2021**, *21*, 2709–2718.
- (26) Iff, O.; Tedeschi, D.; Martín-Sánchez, J.; Moczala-Dusanowska, M.; Tongay, S.; Yumigeta, K.; Taboada-Gutiérrez, J.; Savaresi, M.; Rastelli, A.; Alonso-González, P.; Höfling, S.; Trotta, R.; Schneider, C. Strain-Tunable Single Photon Sources in WSe₂ Monolayers. *Nano Letters* **2019**, *19*, 6931–6936.
- (27) Errando-Herranz, C. et al. Resonance Fluorescence from Waveguide-Coupled, Strain-Localized, Two-Dimensional Quantum Emitters. *ACS Photonics* **2021**, *8*, 1069–1076.
- (28) Kim, J.-H.; Aghaeimeibodi, S.; Carolan, J.; Englund, D.; Waks, E. Hybrid Integration Methods for on-Chip Quantum Photonics. *Optica* **2020**, *7*, 291–308.
- (29) Auksztol, F.; Vella, D.; Verzhbitskiy, I.; Ng, K. F.; Ho, Y. W.; Grieve, J. A.; Viana-Gomes, J.; Eda, G.; Ling, A. Elastomeric Waveguide on-Chip Coupling of an Encapsulated MoS₂ Monolayer. *ACS Photonics* **2019**, *6*, 595–599.
- (30) Pérez-Calixto, D.; Zamarrón-Hernández, D.; Cruz-Ramírez, A.; Hautefeuille, M.; Hernández-Cordero, J.; Velázquez, V.; Grether, M. Fabrication of Large All-PDMS Micropatterned Waveguides for Lab on Chip Integration using a Rapid Prototyping Technique. *Optical Materials Express* **2017**, *7*, 1343–1350.
- (31) Shabahang, S.; Clouser, F.; Shabahang, F.; Yun, S.-H. Single-Mode, 700%-Stretchable, Elastic Optical Fibers Made of Thermoplastic Elastomers. *Advanced Optical Materials* **2021**, *9*, 2100270.

- (32) Kee, J. S.; Poenar, D. P.; Neuzil, P.; Yobas, L. Design and Fabrication of Poly(dimethylsiloxane) Single-Mode Rib Waveguide. *Optics Express* **2009**, *17*, 11739–11746.
- (33) Missinne, J.; Kalathimekkad, S.; Hoe, B. V.; Bosman, E.; Vanfleteren, J.; Steenberge, G. V. Stretchable Optical Waveguides. *Optics Express* **2014**, *22*, 4168–4179.
- (34) Grieve, J. A.; Ng, K. F.; Rodrigues, M. J. L. F.; Viana-Gomes, J.; Ling, A. Mechanically Tunable Integrated Beamsplitters on a Flexible Polymer Platform. *Applied Physics Letters* **2017**, *111*, 211106.
- (35) Schuller, J. A.; Karaveli, S.; Schiros, T.; He, K.; Yang, S.; Kymissis, I.; Shan, J.; Zia, R. Orientation of Luminescent Excitons in Layered Nanomaterials. *Nature Nanotechnology* **2013**, *8*, 271–276.
- (36) Gissibl, T.; Wagner, S.; Sykora, J.; Schmid, M.; Giessen, H. Refractive index measurements of photo-resists for three-dimensional direct laser writing. *Optical Materials Express* **2017**, *7*, 2293–2298.
- (37) Schmid, M.; Ludescher, D.; Giessen, H. Optical properties of photoresists for femtosecond 3D printing: refractive index, extinction, luminescence-dose dependence, aging, heat treatment and comparison between 1-photon and 2-photon exposure. *Optical Materials Express* **2019**, *9*, 4564–4577.
- (38) Luke, K.; Okawachi, Y.; Lamont, M. R. E.; Gaeta, A. L.; Lipson, M. Broadband Mid-Infrared Frequency Comb Generation in a Si_3N_4 Microresonator. *Optics Letters* **2015**, *40*, 4823–4826.
- (39) Malitson, I. H. Interspecimen Comparison of the Refractive Index of Fused Silica. *JOSA* **1965**, *55*, 1205–1209.